Slip velocity has major impact on the frictional strength and microstructure of quartz-muscovite gouges under hydrothermal conditions

André Niemeijer[1,*]
[1] Department of Earth Sciences, Utrecht University, PO Box 80.021, 3508 TA Utrecht, The Netherlands.
a.r.niemeijer@uu.nl

1. Introduction

In order to extrapolate laboratory results of fault gouge strength and stability with some confidence, it is essential to compare experimentally produced microstructures to those observed in exhumed fault zones. However, it is usually not straightforward to directly compare natural and experimental microstructures since 1) natural samples have a complex deformation history of which the PT-conditions and sliding history are typically poorly constrained and 2) friction experiments are necessarily done at a more limited range of sliding velocities (strain rates) than those observed in nature. In addition, the typical aim of friction experiments is to obtain mechanical data such as the stability of sliding (i.e. RSF parameters), which requires varying the sliding velocity, complicating the interpretation of resulting microstructures.
Here, we present the results of rotary shear experiments on simulated fault gouges of 80 wt% quartz and 20 wt% muscovite. Sliding experiments using a four orders of magnitude range of constant velocities (0.03 - 300 μm/s) to a displacement of 30 mm were done at 500 ˚C, 120 MPa effective normal stress and 80 MPa fluid pressure to link the produced microstructure to the observed strength. An additional aim was to reproduce the experimental results obtained in an earlier study on analogue mixtures of salt and muscovite. In those experiments, we found low friction and strong velocity strengthening at low sliding velocity and high friction and mild velocity-weakening at "high" sliding velocity (~ > 5 mm/s). We showed that samples deformed through frictional-viscous flow at low sliding velocity, i.e. through sliding over a weak foliation accomodated by pressure solution of intervening clasts and a competition between time-dependent compaction and displacement-dependent dilation at higher velocity, regulating steady state porosity and thus fricitonal strength.

2. Methods and material

- Artificial gouge mixtures of 80 wt% quartz and 20 wt% muscovite (sil-co-sil 75, d_{mean}=21 μm and crushed optical crystals, d_{mean} = 42 μm)
- Bench thickness of ~1.2 mm
- σ_n^{eff}=120 MPa, P_f = 80 MPa, T = 500 ºC
- Total displacement 30 mm (~γ = 35-45)
- Constant velocity between 0.03-300 μm/s (see Table 1)

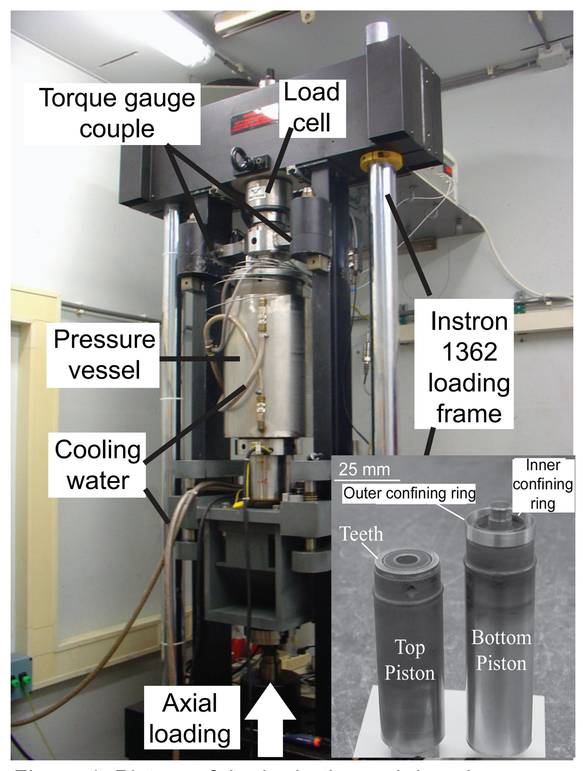

Figure 1: Picture of the hydrothermal ring shear apparatus used in this study. Inset shows the piston set in which the simulated fault gouge is sandwiched. Details are described in Niemeijer et al. (2008).

Table 1:
List of experiments and corresponding parameters
x=displacement, γ = shear strain (displacement / instantaneous layer thickness)
μ = shear stress / normal stress (corrected for seal friction)
** Friction at a shear strain of 2 unless maximum friction is reached before this.*

Experiment	V (μm/s)	x (mm)	γ (-)	μ_{peak}*	μ_{final}	h_{final} (mm)
u192	3	30.387	44.572	0.672	0.878	0.63
u193	30	30.358	36.190	0.650	0.856	0.77
u194	0.3	30.420	40.739	0.755	0.785	0.68
u195	0.03	30.883	38.260	0.651	0.316	0.73
u196	0.1	30.445	42.787	0.690	0.398	0.67
u197	300	30.246	40.054	0.646	0.828	0.69
u198	0.2	30.445	47.911	0.771	0.496	0.59
u199	1	29.715	38.500	0.754	0.870	0.72

3. Mechanical data & models

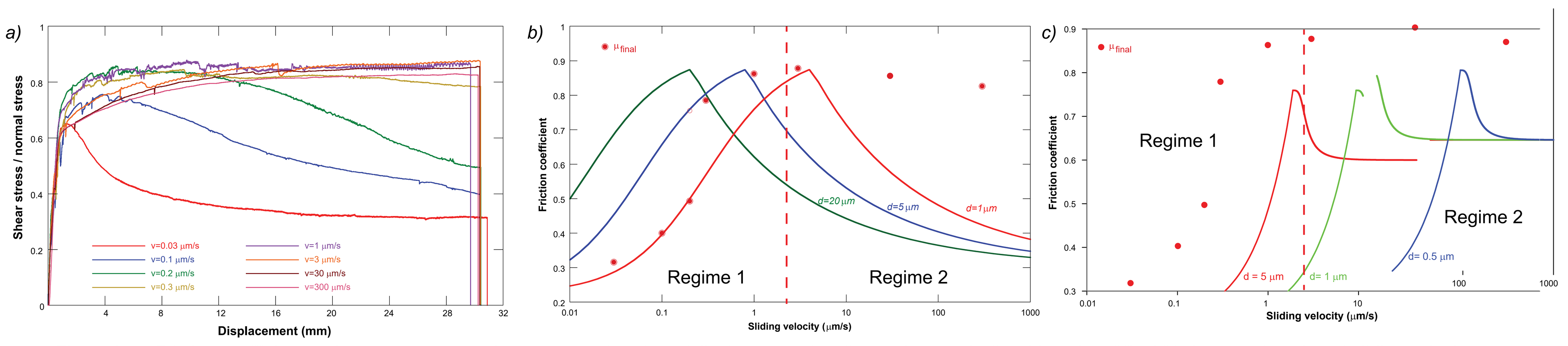

Figure 2. a) Friction coefficient (=shear stress / normal stress) as a function of displacement for all experiments. b) Semi-log plot of final friction as a function of sliding velocity and model predictions for different grain sizes of quartz (Niemeijer and Spiers, 2007) c) same as b) but with the model predictions of Den Hartog (2013). See figure 3 for the microphysical basis of the models.

Regime 1 - Slip on phyllosilicate foliation accommodated by pressure solution of intervening clasts
Regime 2 - Competition between time-dependent compaction and displacement-dependent dilation (granular flow)

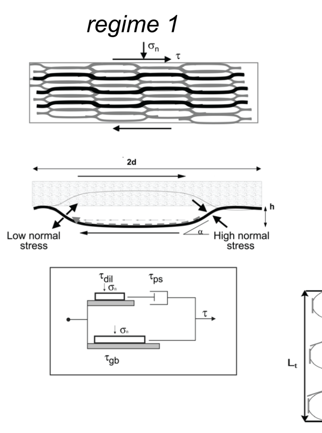

Figure 3 (left)
Schematic diagrams showing the basis for the model predictions shown in Figure 2b.
Model for low (< ~30%) phylloslicate-content mixtures (Niemeijer & Spiers, 2007).
Friction in regime 1 is controlled by the contribution of pressure solution, leading to a strong positive rate-dependence.
In regime 2, friction controlled by the dilatancy angle (i.e. porosity) which in turns is controlled by the competition between compaction and dilation, leading to a strong negative rate-dependence.

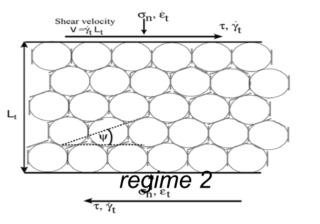

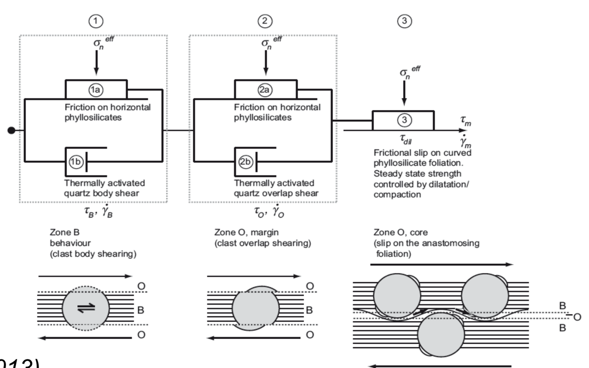

Figure 4 (right)
Schematic diagrams for the model predictions shown in Figure 2c.
Model for high (> 30%) phyllosilicate-content mixtures (Den Hartog, 2013).
In the N&S model, the transition between the two regimes was accomplished through an on/off mechanism depending on the absolute friction predicted by the two parts of the model. In the model of Den Hartog (2013), the transition emerges naturally from the model, leading to a smooth transtion. The difference in the velocity of the transiton between the models is a result of the different dissolution kinetics for quartz used (Rimstidt and Barnes, 1980 in N&S and Tester et al, 1994 in Den Hartog).

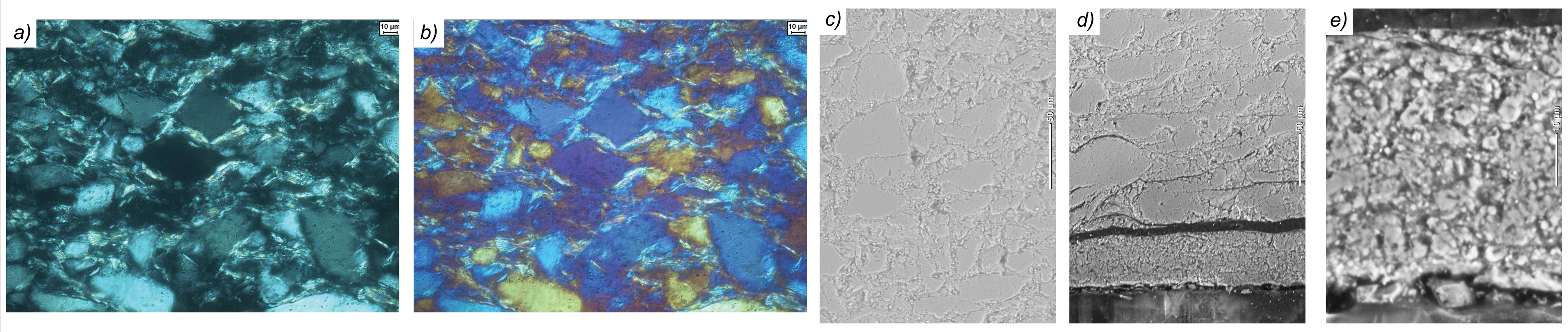

Figure 7: Details of the microstructure of sample u195, deformed at 0.03 μm/s.
Approximate locations of these images are indicated in figure 6.
a) Crossed polars light microscope image of the matrix, showing elongated quartz grains, wrapped by muscovite flakes
b) Same image as a) but with the gypsum plate inserted
c) SEM-BSE image of the matrix showing some larger, elongated quartz clasts. Muscovite is difficult to recognize
d) SEM-BSE of the lower boundary showing a markedly smaller grain size in the boundary shear.
e) Detail of the boundary shear, grain size is 1 μm or smaller.

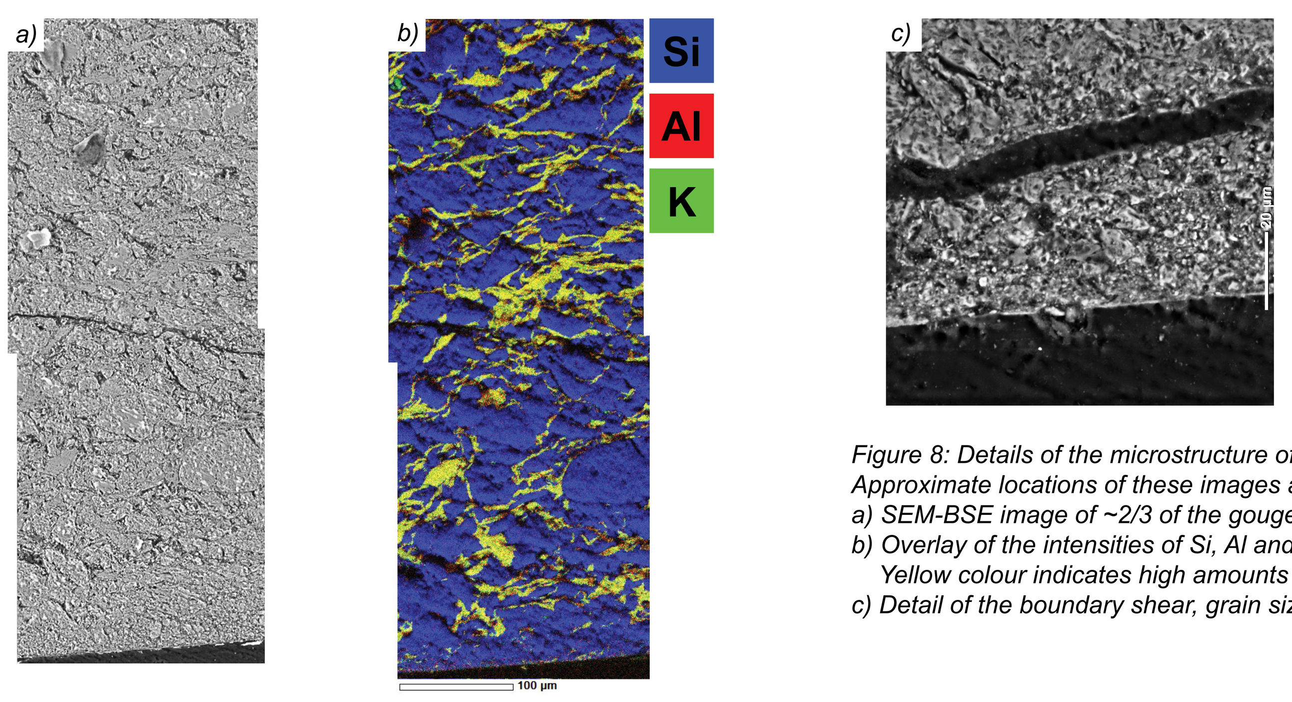

Figure 8: Details of the microstructure of sample u196, deformed at 0.1 μm/s.
Approximate locations of these images are indicated in figure 6.
a) SEM-BSE image of ~2/3 of the gouge width, mapped with EDX
b) Overlay of the intensities of Si, Al and K.
Yellow colour indicates high amounts of Al and K, i.e. muscovite.
c) Detail of the boundary shear, grain size is 1 μm or smaller.

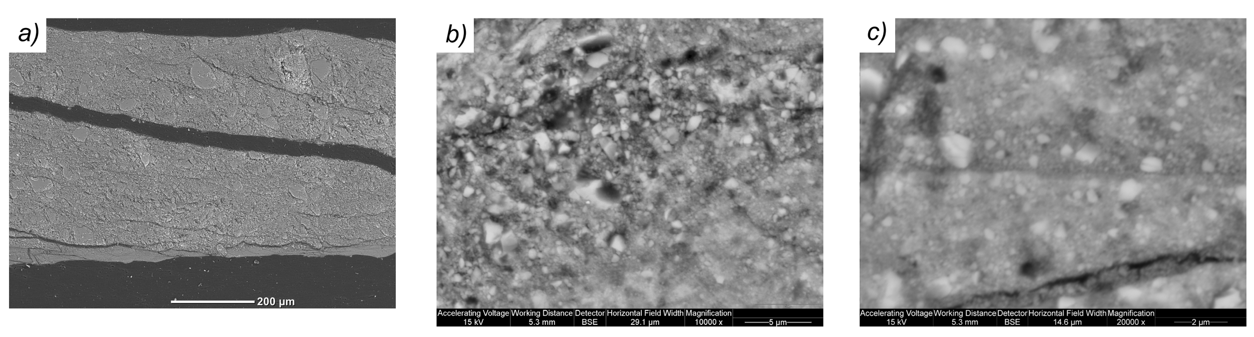

Figure 9: Details of the microstructure of samples u194 and 192, sheared at 0.3 and 3 μm/s, respectively.
Approximate locations of these images are indicated in figure 6.
a) SEM-BSE image of sample u194. The boundary shear band can be clearly distinguished due to the fine grain size.
b) Detail of the boundary shear in u192, grains much smaller than 1 μm are visible.
c) Further of detail of the boundary shear in u192, smallest grains distinguishable might be 0.1 μm

Low velocity:
- Anastomosing muscovite foliation with intervening quartz clasts

All velocities:
- Boundary zone of very fine grain size (< 1 μm).
- Increasing zone thickness with increasing velocity.
- Zone is characterized by a uniform extinction (CPO in quartz ?)

4. Microstructual Observations

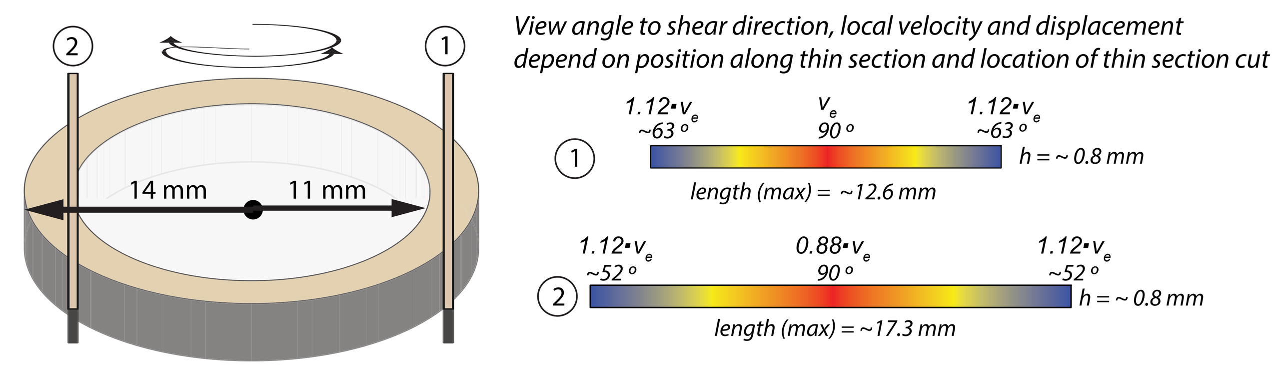

Figure 5: Schematic representation of the location of the thin section cuts, variation of the angle of view with respect to the shear direction, sliding velocity and displacement.

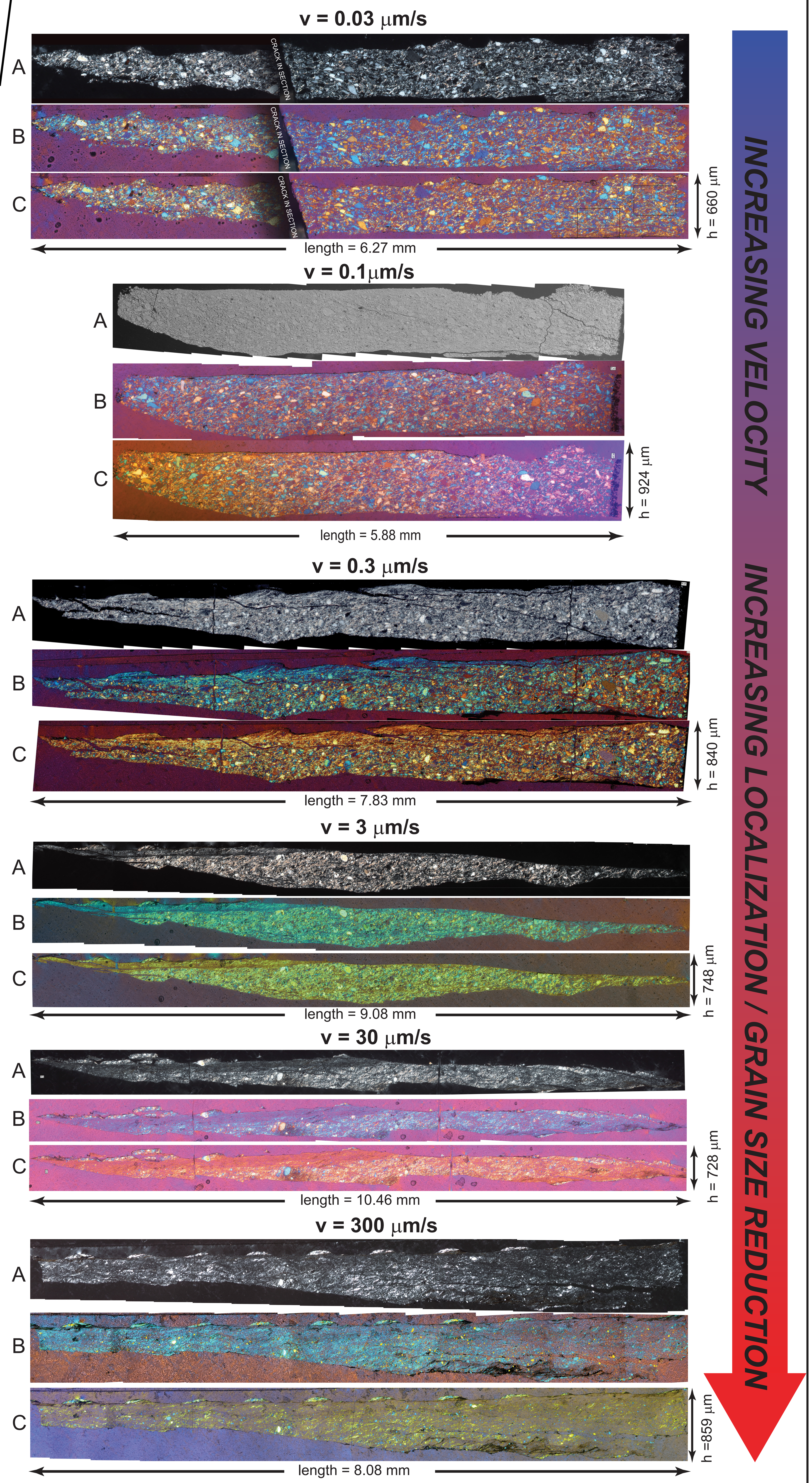

Figure 6: Mosaics of the microstructure after 30 mm of displacement for 6 different sliding velocities.
Panel A is from images taken with a polarizing light microscope with crossed polars (with the exception of 3.2a, which is from SEM-BSE images), panels B and C are with the gypsum plate inserted but rotated 90 º with respect to each other. Shear sense is dextral in all panels.

5. Conclusions and open questions

- Quartz/muscovite fault gouges show a large variation in frictional strength with sliding velocity
- Localized grain size reduction occurs at all velocities, accompanied by uniform extinction, indicating a CPO.
- Models reproduce low velocity, strengthening regime reasonably well.
- Mild velocity-weakening at high velocity not reproduced => effect of localized grain size reduction ?
- Need for constant velocity experiments to various strains to link friction to microstructures.

References
Rimstidt and Barnes, Geochimica e Cosmochimica Acta, vol. 40, pp. 1683-1699, **1980** .
Niemeijer and Spiers, Geological Society of London, Spec. Publ. 245, pp. 303-327, **2005.**
Niemeijer and Spiers, Journal of Geophysical Research, vol. 112, B10405, **2007.**
Den Hartog, Utrecht Studies in Earth Sciences, PhD thesis, 178 pages, **2013.**
Tester, Worley, Robinson, Grigsby and Feerer, Geochimica e Cosmochimica Acta, vol. 58, pp.2407-2420, **1994.**
Niemeijer and Spiers, Tectonophysics, vol. 427, pp. 231-253, **2006.**
Niemeijer, Spiers and Peach, Tectonophysics, vol. 460, pp. 288-303, **2008.**